JOURNAL OF THERMOPHYSICS AND HEAT TRANSFER
Vol. 20, No. 4, October–December 2006

Two-Dimensional Conduction Effects in Estimating Radiative Flux from a Capillary Discharge

Malay K. Das* and Stefan T. Thynell†
The Pennsylvania State University, University Park, Pennsylvania 16802

DOI: 10.2514/1.23158

It is quite common to employ thin metallic films for the determination of heat flux at a fluid–solid interface. Depending on the duration of the event and gage design, it may be important to account for multidimensional heat conduction within the thin-film substrate. Present work investigates the effects of two-dimensional conduction on the deduced radiative heat fluxes using an inverse algorithm. For comparison, a previously developed one-dimensional inverse technique is also used. The high heat fluxes are produced by an electrothermal–chemical plasma jet. The plasma, initiated within a 3.2 mm diameter and 26 mm long polyethylene capillary by exploding a 3.6 mg thin copper wire, emerges into an open-air atmosphere as an underexpanded supersonic jet. The jet impinges over a stagnation plate equipped with thin-film platinum gages, whose temperature history serves as an input to the heat-flux estimation algorithm. Four different charging voltage levels are investigated, ranging from 2.5 to 7.5 kV. While both algorithms capture the temporal variations of the radiative heat fluxes, the two-dimensional model reveals the discrepancies between the two techniques, as well as the range of applicability of the one-dimensional model.

Nomenclature

c	=	specific heat, J/kg K
d	=	domain length in y direction, m
e	=	relative difference between 1-D and 2-D estimations
j	=	iteration number
k	=	conductivity, W/m K
l	=	domain length in x direction, m
q''	=	heat flux, W/m^2
T	=	temperature, K
t	=	time, s
w	=	half-width of gage, m
x, y	=	Cartesian coordinate directions
Y	=	measured temperature, K
α	=	thermal diffusivity, m^2/s
Γ	=	confidence interval
θ	=	nondimensional temperature
ρ	=	density, kg/m^3
σ	=	standard deviation
τ	=	nondimensional time (Fourier number)

Superscripts

j	=	iteration number
*	=	nondimensional

Subscripts

f	=	final
max	=	maximum
ref	=	ambient

Received 12 February 2006; revision received 10 April 2006; accepted for publication 10 April 2006.

*Research Assistant, Department of Mechanical and Nuclear Engineering. Student Member AIAA.

†Professor, Department of Mechanical and Nuclear Engineering. Associate Fellow AIAA.

Introduction

TRANSIENT heat-flux estimation typically employs surface temperature measurements followed by a suitable data-reduction scheme [1,2]. These schemes often use the measured temperature as a boundary condition, solve the heat conduction problem numerically, and estimate the temperature gradient at the surface. This procedure relies on the availability of a noise-free and a continuous boundary temperature [3,4]. Experimental data, being neither exact nor continuous, impose two-way instability in the solution. First, differentiation of the finite-precision experimental data sensitizes the estimated heat flux to measurement uncertainties causing solution instabilities [5,6]. Second, ill-posedness caused by the discreteness of the experimental data introduces nonuniqueness in the heat-flux estimation [7,8]. While solution uniqueness can be influenced by the amount of acquired data, solution stability can only be achieved by a suitable mathematical treatment. Over the years, several techniques have been developed to deal with this stability issue. These techniques include the following: smoothing of either the discrete measurement data or the derivatives [5,9], higher-order finite-difference schemes [10], filtering techniques [11–13] as well as inverse estimation technique [3]. The inverse-based approach has shown several attractive benefits over other numerical techniques [3].

Inverse techniques, when implemented properly, can efficiently use experimental data. Except for a few simple and mostly one-dimensional (1-D) cases, where inverse problems can be solved analytically, the inverse procedure usually starts with a reasonable guess, solves a direct problem, and forms a suitable functional using the difference between the calculated and the measured data. The functional is then gradually optimized by an iterative improvement of the initial guess. Solution instability, caused by measurement noise, is circumvented by regularization. Regularization typically sets a stopping criterion for the optimization algorithm preventing minimization of the functional and thus insulates the final solution from the measurement noise. Inverse techniques can implement optimization and regularization in different ways. Early theories of inverse heat transfer problems, developed by Beck et al. [7], Alifanov [8], and Tikonov et al. [14] are now further extended and extensively applied by several authors including Ozisik and Orlande [15]. Inverse techniques were successfully implemented in conduction [16], convection [17], radiation [18], thermophysical property determination [19], as well as hyperbolic heat conduction [20] problems. In conduction heat transfer, inverse techniques can be used to recover unknown boundary or initial conditions [21]. Estimation of boundary conditions requires accurate information of thermophysical

properties, temperature measurement within a region that is extremely sensitive to the unknown boundary condition, a suitable optimization algorithm as well as an effective regularization procedure to impose stability. Determination of unknown heat fluxes from surface temperature measurements at discrete time intervals can thus be modeled as an inverse conduction problem with unknown boundary conditions.

Taler [2] formulated an inverse heat conduction problem for estimating transient heat flux from surface temperature measurement using three different sensors: thin-film gage, thick-wall gage, and thin-skin calorimeter. A 1-D inverse conduction model was employed to estimate the transient heat flux by the Stefan–Burggraf–Langford method. A smoothing technique, utilizing cubic spline or digital filtering, restricted the instability caused by measurement noise. The data-reduction complexity, however, was compensated by an accurate and computationally efficient heat-flux estimation. Bezuidenhout and Schetz [22], Mota et al. [23] and Das et al. [24,25] also successfully implemented inverse techniques in estimating surface heat fluxes.

Walker and Scott [3] extensively studied and compared different transient heat-flux estimation techniques using surface temperature measurements. They arranged available methodologies in three different groups: analytical, direct numerical and inverse techniques. 1-D conduction problems were formulated assuming typical transient variations of the surface heat flux. Based on a rigorous quantitative error analysis, it was concluded that inverse techniques, when properly regularized, provide the most accurate and stable solutions.

Despite the accuracy and stability of inverse heat-flux estimation techniques, the assumption of one-dimensionality restricts their applicability. A deep thermal wave penetration coupled with, for example, a highly localized heat flux imposed externally or imposed by the gage itself, may produce a substantial departure from one-dimensionality. Smith et al. [26] employed a two-dimensional (2-D) numerical model to examine the validity of 1-D assumption for heat-flux measurements in a gas-turbine application using thin-film gauges. Walker et al. [27,28] discussed a 2-D inverse approach and compared its performance with a 1-D technique in estimating heat fluxes during a shock–shock interaction. Following an earlier effort [29], they used a function specification method with suitable regularization. Using quantitative error estimation, it was concluded that the 2-D approach resolves steep spatial gradients of heat fluxes more accurately than the 1-D technique.

Large heat-flux levels occur during electrothermal–chemical (ETC) ignition of solid propellants. The ignition source is a high-temperature, high-pressure, metal-wire initiated, hydrocarbon capillary-sustained plasma jet. ETC ignition has confirmed its effectiveness over conventional chemical ignition methods [30–38], yet understanding of its complexity is only now beginning to emerge. Radiation constitutes one of the principal energy transport mechanism in ETC ignition [39]. Efforts of quantifying the relative importance of different energy transport mechanisms, therefore, include measurement and computation of transient radiative heat flux [24,25,40–47].

Measurement of radiant heat fluxes from an ETC plasma jet is often based on jet impingement on a surface, whose transient temperature is recorded via a surface-mounted thin film. The measured temperature serves as an input to a 1-D inverse data-reduction scheme for heat-flux calculation [24,25]. Surface temperatures are typically measured by narrow thin-film metallic gages placed on a low thermal conductivity substrate. The gage, connected with a constant current source, records the substrate's surface temperature. Assuming 1-D heat conduction within the substrate below the gage with an unknown heat flux at one boundary and semi-infinite boundary condition at the other, an inverse conduction problem is formulated and solved. Despite the success of this technique when applied to low heat-flux levels, high heat-flux measurements require a substrate with a much higher thermal diffusivity to prevent gage failure due to excessive temperatures. Since the thermal wave penetration depth may be comparable to the gage width, the assumption of 1-D heat conduction in the substrate may be inaccurate. The data-reduction procedure should, therefore, be critically examined and suitably devised to address this issue.

The present study considers 2-D heat conduction within the substrate of surface-mounted thin-film gages subjected to high radiant heat fluxes from an ETC plasma jet. The computational–experimental approach is described, and results from 1-D and 2-D inverse conduction techniques are compared. Experimental procedures and 1-D formulation uses a previously described procedure [24,25]. In this work, the thin-film platinum gages are mounted on polyimide or sapphire substrate, depending on the plasma energy levels. Narrow thin-film gages, coupled with high thermal conductivity and diffusivity of sapphire, may require consideration to 2-D heat conduction within the substrate. The study also investigates possible parameters influencing the 2-D effect within the substrate.

Experimental Apparatus and Approach

Plasma Generator

The pulse forming network (PFN) used for plasma initiation is discussed elsewhere in detail [24,25]. The PFN can be charged up to 10 kV to yield a maximum energy storage of 9.6 kJ. For the present experiment, four different voltage levels are studied: 2.5, 4, 5 and 7.5 kV (0.60, 1.54, 2.40, and 5.40 kJ, respectively). The plasma chamber consists of a capillary, a fine copper wire, Elkonite (copper–tungsten alloy: 30% Cu, 70% W) electrodes, and other nonconducting housing hardware. After being established, the plasma flows through an Elkonite nozzle into the ambient open-air environment. Once evolved from the nozzle, the plasma impinges on a stagnation plate located at a distance of 50 mm from the nozzle exit. Heat-flux gages, covered by fused-silica windows, are placed on the stagnation plate. The details of gauge locations and window effects are discussed elsewhere [24].

Heat-Flux Gage Design

Thin-film platinum (80 nm thick) sputtered on polyimide (50 μm thick) was used for deducing the transient variation of the radiative heat flux for a 2.5 kV charging voltage. For higher charging voltages, platinum (80 nm) was sputtered on sapphire (500 μm thick). These gages are 0.25 mm wide and 12 mm long, suggesting that three-dimensional heat conduction effects are not important. A National Semiconductor's LM134 constant current source, set at 3 mA, powered by a 9 V battery, is connected to the platinum gauge via 500 nm thick sputtered copper leads. The gage was attached to a SS304 substrate through a transfer tape. Additional details are available [24].

Data Reduction

A standard 1-D inverse approach, for which a semianalytical solution is available, estimates the transient, absorbed radiative heat-flux variation from the measured time-dependent surface temperatures. The model assumes that conductive transfer in the substrate is 1-D, that a perfect thermal contact is made between the platinum film and the substrate, and that thermophysical properties are constant. Based on the inverse approach described in detail by Ozisik [15], a numerical procedure was developed. The governing equation along with the initial and boundary conditions are discussed elsewhere [24,25].

The 2-D inverse data-reduction technique discussed here is developed around a conjugate-gradient optimization procedure. A typical conjugate-gradient algorithm starts with a steepest descent scheme followed by a coupling of present and previous descent directions through a conjugate coefficient [48–50]. This technique, when applied to inverse conduction problems, generates three partial-differential equations namely, direct, adjoint, and sensitivity [51], along with appropriate initial and boundary conditions. The solution starts from an initial guess of the unknown. A suitably defined functional, incorporating the measured and computed data, is then iteratively optimized by adding a gradual correction to the initial guess. Adjoint and sensitivity equations are solved to determine this

correction. The adjoint equation calculates the gradient of the functional, which in turn determines the descent direction. The sensitivity equation uses the gradient to deduce the descent step size. In each iteration, all three equations are solved to generate a correction based on the descent direction and step size. Iterations proceed until the convergence criterion set by the regularization scheme is met [8,15,52].

In the present case, the 2-D inverse technique solves the following partial-differential equation:

$$k\left(\frac{\partial^2 T}{\partial x^2}+\frac{\partial^2 T}{\partial y^2}\right)=\rho c\frac{\partial T}{\partial t} \tag{1}$$

$$-k\frac{\partial T}{\partial x}=\begin{cases} q''(t) & \text{at } x=0,\ 0\le y\le w \\ 0 & \text{at } x=0,\ w<y\le d \end{cases} \tag{2a}$$

$$T=T_{\text{ref}} \quad \text{at } x\to\infty,\ t=0 \tag{2b}$$

$$\frac{\partial T}{\partial y}=0 \quad \text{at } y=0,\ d,\ 0<x<\infty \tag{2c}$$

$$q''(t)=\begin{cases} q^{j-1} & \text{at } x=0,\ 0\le y\le w \\ 0 & \text{at } x=0,\ w<y\le d \end{cases} \tag{2d}$$

where q^{j-1} is the updated heat flux after the $(j-1)$-th iteration. For the first iteration, $q''(t)$ represents the initial guess of the unknown heat flux. The above equations can be posed in the following dimensionless form:

$$\frac{\partial^2\theta}{\partial x^{*2}}+\frac{\partial^2\theta}{\partial y^{*2}}=\frac{\partial\theta}{\partial\tau}$$
$$\text{for } 0<x^*<\infty, \qquad 0<y^*<\infty, \qquad 0<\tau<\tau_f \tag{3}$$

$$-\frac{\partial\theta}{\partial x^*}=\begin{cases} q^*(\tau) & \text{at } x^*=0,\ 0\le y^*\le w^* \\ 0 & \text{at } x^*=0,\ w^*<y^*\le 1 \end{cases} \quad \text{at } x^*=0 \tag{4a}$$

$$\frac{\partial\theta}{\partial y^*}=0 \quad \text{at } y^*=0,1, \qquad 0<x^*<\infty \tag{4b}$$

$$\theta=0 \quad \text{at } x^*\to\infty \tag{4c}$$

$$\theta=0 \quad \text{at } \tau=0 \tag{4d}$$

where $x^*=x/d$, $\tau=(\alpha t)/d^2$, $\theta=(T-T_{\text{ref}})/T_{\text{ref}}$, $q^*(\tau)=q''(t)d/(kT_{\text{ref}})$, and $\alpha=k/(\rho c)$; w^* is the dimensionless gage half-width. Equation (3), along with the above initial and boundary conditions, describes only the direct problem. The solution to the subsequent sensitivity and adjoint problems is obtained by using a standard conjugate-gradient technique and is discussed elsewhere [49,53]. The solution is regularized through the discrepancy principle [8,15]. The discrepancy principle terminates the iteration when the difference between computed and measured temperature reaches the standard deviation (σ) of the measurement. While using experimental data, where σ may vary from point to point, an average value of σ is used.

Figure 1 shows the solution domain and the governing equation along with the boundary conditions. Considering the symmetry of the problem, the solution domain is restricted to half of the physical domain, that is, $y=0$ is the symmetry axis. Radiative flux is absorbed by the gage located between $y=0$ to $y=w$, over which the flux is assumed to be spatially uniform. It is also assumed that the substrate either reflects or transmits the radiative heat flux that arrives between $y=w$ to $y=d$, keeping $w<y<d$ virtually insulated. Symmetry and zero flux are assumed along midplane at $y=0$ and at $y=d$, respectively, whereas semi-infiniteness contributes the boundary condition as $x\to\infty$. The solution domain remains the same for the direct, adjoint, and sensitivity problems; the governing equations and boundary conditions are, however, changed in each problem. Additionally, to impose the condition of heat-flux uniformity over the gage and an insulated surface elsewhere, the gradient is averaged over the gage width and forced to zero elsewhere.

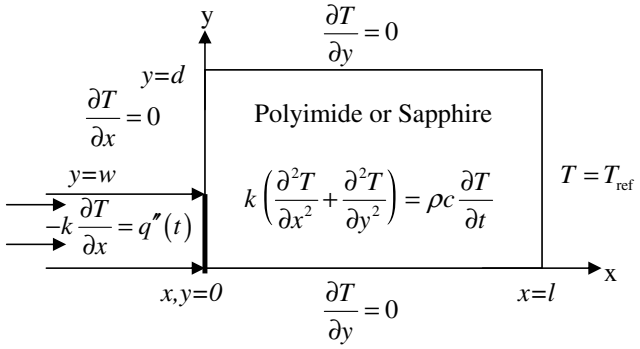

Fig. 1 Solution domain, governing equation and boundary conditions for the direct problem of the two-dimensional inverse data-reduction model.

Solution Methodology

Intermediate steps of the 2-D inverse technique require numerical solution of partial-differential equations using the deduced initial and boundary conditions. The solution domain (Fig. 1) is discreteized using a fully implicit finite-difference scheme. The alternate direction implicit technique, followed by tridiagonal matrix inversion by the Thomas algorithm, is then used [54].

Grid independence of the numerical solution is tested against three different grid sizes: 51×51, 101×101, 201×201. A 101×101 grid size is selected finally as further refining produces negligible improvement of the solution. Nonuniform grids are used, keeping denser grids near $x=0$ and $y=0$ lines, followed by stretching of grid size in geometric progression. The time step is maintained below one-tenth of the minimum specified by grid Fourier number criteria [51].

For the validity of semi-infinite solid assumption, boundary condition as $x\to\infty$ should satisfy the relation: $x\ge 4\sqrt{\alpha t_f}$ [55], which for the nondimensional equations becomes $x^*\ge 4\sqrt{\tau}$. Present solution maintained $x^*\ge 5\sqrt{\tau}$ for all cases. In addition to numerically generated temperature profile, the simulations also use experimental data from the heat-flux gages exposed to plasma jet of varying energy levels. The heat-flux gage width is 250 μm and distance between two consecutive gages is 9.5 mm; $y=w$ is set at 125 μm and $y=d$ at 500 μm, as a larger value of d failed to produce any appreciable improvement in estimation.

The CPU time for the 1-D problem is around 1.5 min for 501 input data points, when using a 3.6 GHz P4 computer with 512 MB SDRAM and LINUX operating system. CPU time for the 2-D problem depends upon the initial guess. Using the 1-D solution as a first guess, the CPU time is about 5 min. Starting from a random guess, the computing time may rise up to 30 min.

Thermophysical Properties

The temperature coefficient of the electrical resistivity of platinum was assumed to be linear over the temperature range from 20 to 250°C, and was measured as 0.002/K using a standard convection oven. This value is about 50% lower than the bulk value (0.00389/K). The thermophysical properties of substrates are tabulated in Table 1. The normal polyimide conductivity obtained by Kurabayashi et al. [56] is used here, and other data were obtained from the manufacturer's manual.[‡]

[‡]http://www.goodfellow.com [cited 29 April 2005].

Table 1 Thermophysical properties of substrate materials

Substrate material	ρ(kg/m^3)	c(J/kg-K)	k(W/m-K)
Polyimide	1420	1040	0.25
Sapphire	3985	750	37.50

Discussion of Results

Figure 2 illustrates the accuracy of the developed 1-D and 2-D inverse techniques in estimating the unknown surface heat flux based on numerically generated input data. For these results, the 2-D direct problem is solved with a known surface heat flux at $x^* = 0$, semi-infinite condition as $x^* \to \infty$ and insulated boundaries at $y^* = 0$ and $y^* = 1$. The heat-flux profile at $x^* = 0$ is maintained as

$$q^* = 1.0 \quad \text{for } 0 \le y^* \le 1 \tag{5}$$

The direct problem determines the transient surface temperature data that serve as the input to the inverse algorithms for the heat-flux reconstruction. The 2-D direct problem is solved keeping only few cells in a y direction, thus producing a 1-D temperature profile. The computed surface temperatures are assumed as exact data generated from an idealized experiment. Clearly, for this particular formulation no formal regularization is required, and the inverse problem reduces only to the minimization of the relevant functional. Simulating with a steady and spatially uniform heat flux, it is readily observed that both 1-D and 2-D inverse techniques estimate the heat flux accurately irrespective of the substrate material. Both formulations produce similar results here, as the problem itself is essentially one-dimensional.

The accuracy of any inverse approach, however, diminishes rapidly with the introduction of noise in the input data. To illustrate the performance of inverse techniques with noisy data, a Gaussian noise is imposed over the exact data. For this purpose, Gaussian random numbers of specified mean and standard deviations are generated from the random number generation function provided within a standard high-level computer language. A Box–Muller scheme is used for this purpose [57]. The zero-mean random numbers are then used to perturb the simulated experimental data in the following manner:

$$Y^*(\text{perturbed}) = Y^*(\text{exact}) \pm \Gamma\sigma \tag{6}$$

where $Y^* = (Y - T_{\text{ref}})/T_{\text{ref}}$, σ denotes the standard deviation of the Gaussian distribution, and Γ indicates the confidence interval, which is set here as 2.576 to specify 99% confidence. The results of the simulations are shown in Fig. 3 with an assumed heat-flux profile of

$$q^*(\tau) = 4.0\tau(1 - \tau) \quad \text{for } 0 \le y^* \le 1 \tag{7}$$

Solving the 2-D direct and inverse problems using the discrepancy principle as iteration stopping criterion, it is readily observed that the estimation deviates from the exact with the incorporation of the simulated measurement noise. However, if the discrepancy principle is rejected altogether and the functional is minimized toward zero, the inherent instability of the inverse problem produces an unbounded error as shown in Fig. 3.

Figures 2 and 3 proved the effectiveness of 1-D and 2-D inverse techniques in recovering spatially uniform unknown heat fluxes. Results from 1-D and 2-D techniques coincide in these cases. Practical applications, however, often encounter spatially varying heat-flux profiles creating a 2-D temperature field within the substrate. Two-dimensional algorithms are thus required in these cases. Case studies in Fig. 4 show the results of imposing nonuniform dimensionless heat-flux profiles A and B in Table 2. The solution starts by solving the 2-D direct problem [Eqs. (3) and (4)] with the given heat-flux profiles. The temperature profiles at $x^* = 0$ thus obtained are used as the input to the inverse algorithms. The 1-D and 2-D inverse problems are then solved to recover the surface heat fluxes. No measurement noise is imposed, that is, the functional is minimized without premature stopping. A w^* of 0.25 is maintained for both 2-D direct and inverse problems. As illustrated in Fig. 4, the results show appreciable deviation of the 1-D from the exact solution as time progresses. The 2-D formulation, however, accurately recovers the original heat fluxes. The 2-D formulation, used in the present investigation, deviates from the standard conjugate-gradient technique [15] in terms of spatial averaging and allowing evolution of certain variables only at specified regions. Figure 4, therefore, in addition of showing the limitation of the 1-D technique, validates the 2-D algorithm as well.

Figures 5–8 illustrate the performance of 1-D and 2-D algorithms in reconstructing the radiant heat flux from the hydrocarbon capillary-sustained plasma jet. Four different plasma charging voltage levels are studied: 2.5, 4.0, 5.0, and 7.5 kV (0.6, 1.5, 2.4, and 5.4 kJ of energy, respectively). The 2.5 kV case uses a polyimide substrate, whereas the other cases use a sapphire substrate. The temperature profile, used as the input to the inverse algorithm, is also

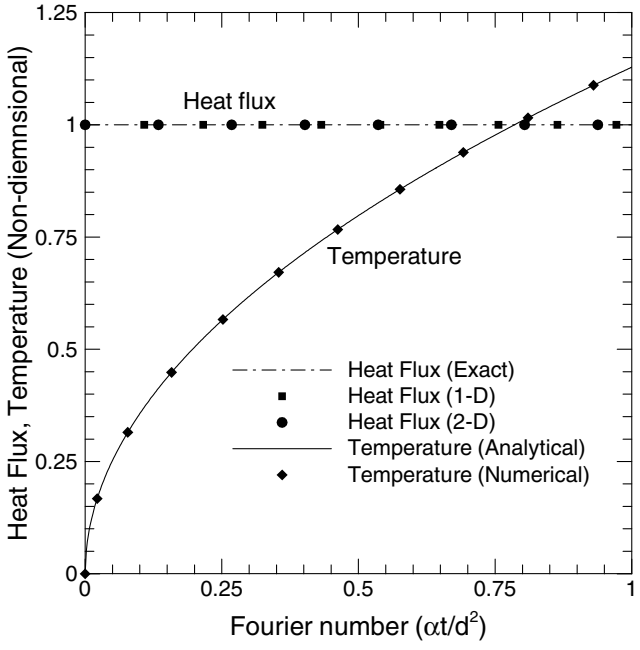

Fig. 2 Validation of the direct and inverse solution using an assumed heat-flux constant.

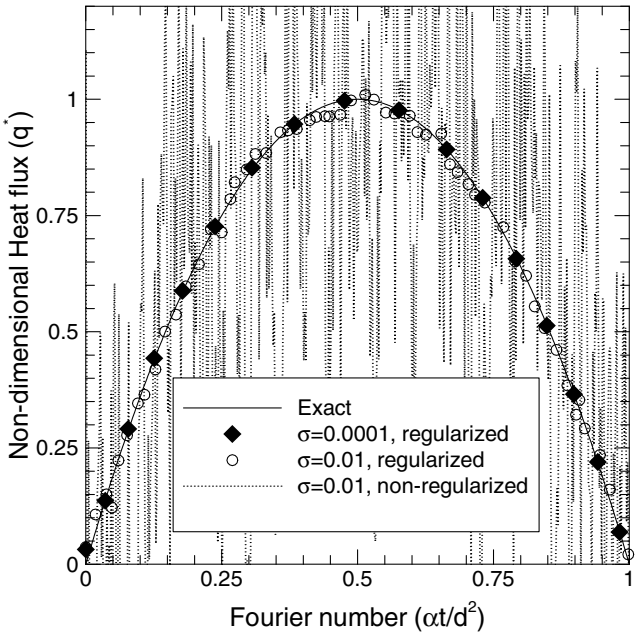

Fig. 3 Performance of two-dimensional inverse algorithm with noisy temperature data [Eq. (6)].

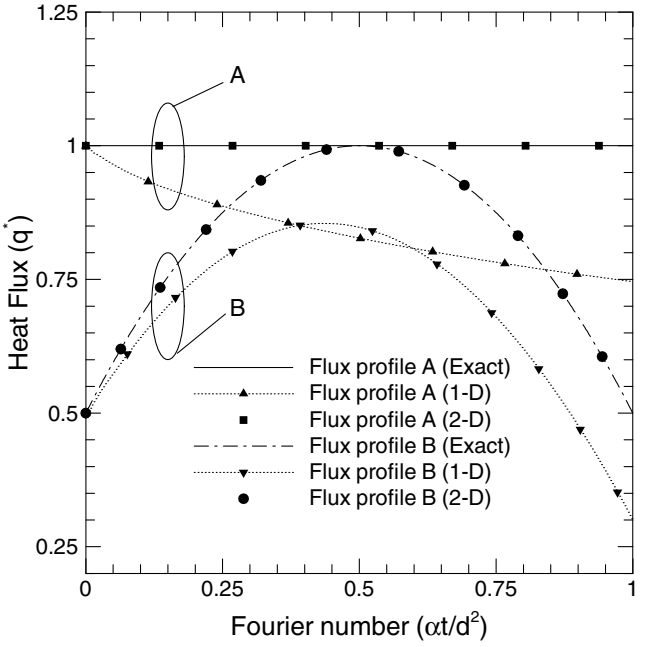

Fig. 4 Performance of one- and two-dimensional inverse techniques with spatially varying flux profiles.

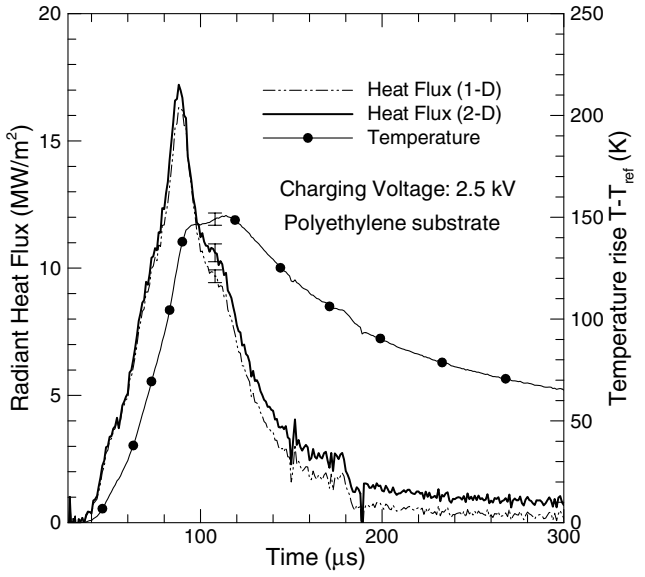

Fig. 5 Performance of one- and two-dimensional inverse data-reduction approach for estimating radiant heat flux from a 2.5 kV capillary plasma.

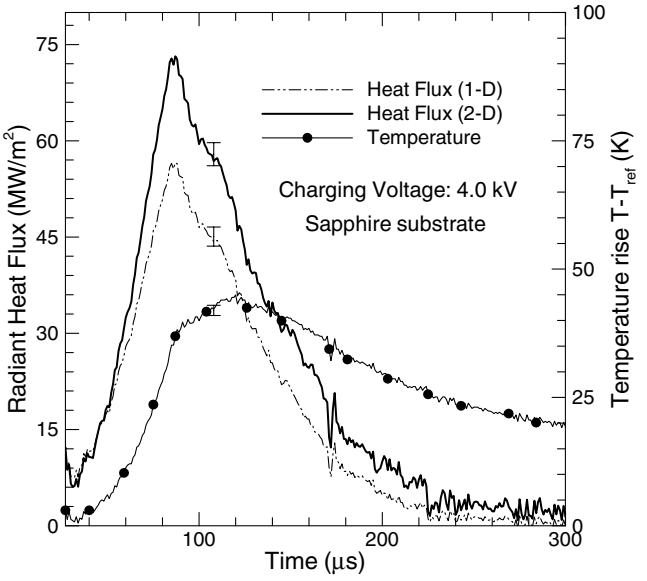

Fig. 6 Performance of one- and two-dimensional inverse data-reduction approach for estimating radiant heat flux from a 4.0 kV capillary plasma.

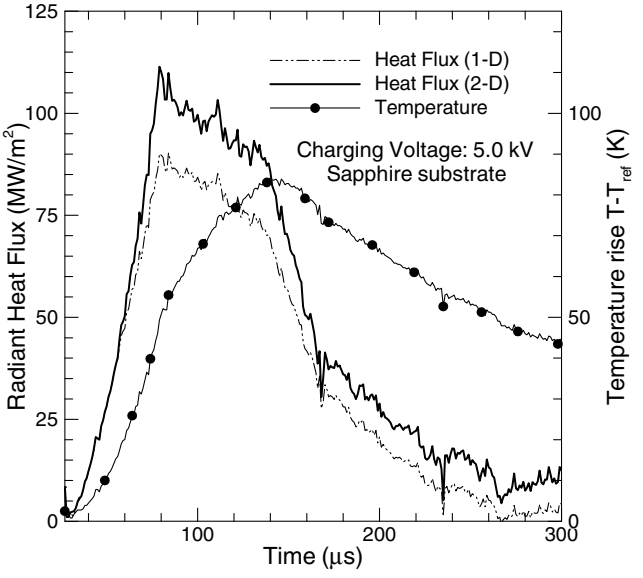

Fig. 7 Performance of one- and two-dimensional inverse data-reduction approach for estimating radiant heat flux from a 5.0 kV capillary plasma.

shown in the plots. For convenient comparison with previous works [24,25], plots are presented in dimensional form. Error bars placed at $\pm 2\sigma$ indicate the uncertainties in the experiment and data reduction, where σ is the standard deviation from three repeated experiments. The differences between 1-D and 2-D estimations are calculated; a parameter e, the relative estimation error, is defined below and its values are tabulated in Table 2.

$$e = \left| \frac{q''(2-D) - q''(1-D)}{q''(2-D)} \right| \times 100\% \tag{8}$$

The sapphire substrate exhibited substantial deviation (25%), while negligible 2-D effect observed in polyimide (6%). Table 3 indicates weaker dependence of e with plasma energy levels than substrate material properties. Average e also exceeds e at maximum heat-flux location in all experiments, indicating maximum e does not coincide with maximum heat-flux level. Additionally, it is important to observe that both the 1-D and the 2-D formulations do recover the fluctuating components of the transient radiative heat flux. This is clearly revealed in Fig. 8. The fluctuating components are largely caused by the highly compressible nature of the underexpanded supersonic jet and its interaction with the stagnation plate.

While both algorithms recover the essential transient features, the nature of the 2-D effect requires further investigation. The 2-D effect implies lateral (y-directional) heat conduction, which is neglected in the 1-D formulation. Lateral conduction in sapphire exceeds that of polyimide due to about 100-fold increase in thermal diffusivity of the former (Table 1). The very property that suggested the use of sapphire for high heat-flux measurements contributes to its higher 2-D effect as well. An optimum design of heat-flux measurement experiment, therefore, requires identification of all possible parameters and their relative roles in contributing to the 2-D effect. The nondimensional governing equations [Eqs. (3) and (4)] suggest that for noise-free input data, the estimated heat fluxes and consequently the 2-D effect will depend only upon τ, $\tau_{\max}$, q^*, and w^*. To investigate the relative roles of these parameters on e, a series

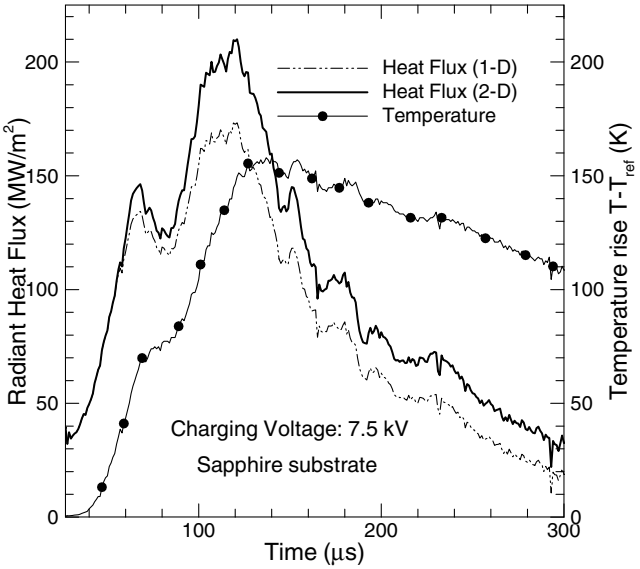

Fig. 8 Performance of one- and two-dimensional inverse data-reduction approach for estimating radiant heat flux from a 7.5 kV capillary plasma.

of numerical experiments are performed imposing different flux profiles, gage widths, and maximum Fourier numbers. Temperature profiles generated from the 2-D direct problem are used as noise-free input to both 1-D and 2-D inverse problems. Resulting 2-D effects are calculated using Eq. (8) replacing q'' by q^*.

Figures 9a and 9b show the variation of the relative heat-flux error e with w^* and τ for flux profiles A and B of Table 2 with a fixed τ_{max} of 1.0. The figures clearly reveal nonlinear increase of e with increasing τ and decreasing w^*. For the parabolic flux profile (B), e maintains a moderate gradient up to about $\tau = 0.50\tau_{max}$ and rises sharply for $\tau > 0.50\tau_{max}$. This sharp rise can be correlated to the decreasing trend in flux level in that interval. Figure 4 shows for profile B that after $\tau = 0.50\tau_{max}$, the difference between 1-D and 2-D estimations remains almost constant. The heat flux itself, however, decreases. Consequently, the 2-D estimation delivers a very high e that may increase to a large value if the flux approaches a very low value at $\tau = \tau_{max}$. Nevertheless, in the interval $\tau \leq 0.50\tau_{max}$ the difference of e from flux profiles A and B remains within about 10%. The 2-D effect, therefore, tends to increase exponentially with

Table 2 Different heat-flux profiles used in simulations; $q^* = 0$ for $w^* < y^* \leq 1$ in all cases

Flux profile	$q^*(\tau)$ at $x^* = 0, 0 < y^* \leq w^*$
A	1.0
B	$0.50 + 2.0\frac{\tau}{\tau_{max}}(1 - \frac{\tau}{\tau_{max}})$
C	$0.50 - \tau(1 - 0.50\tau)$
D	$0.50(1 - \tau)$
E	$0.50(1 - \tau^2)$
F	$0.50(1 + \tau^2)$
G	$0.50(1 + \tau)$
H	$0.50 + \tau(1 - 0.50\tau)$

Table 3 Relative difference between the 1-D and 2-D algorithms in estimated heat fluxes for different charging voltages and substrate materials

Charging voltage (kV)	Substrate material	e at peak heat-flux location (%)	e averaged over 0 to 500 μs, e_{av}, (%)
2.5	Polyimide	5.23	7.65
4.0	Sapphire	22.60	33.24
5.0	Sapphire	19.14	31.11
7.5	Sapphire	17.47	21.02

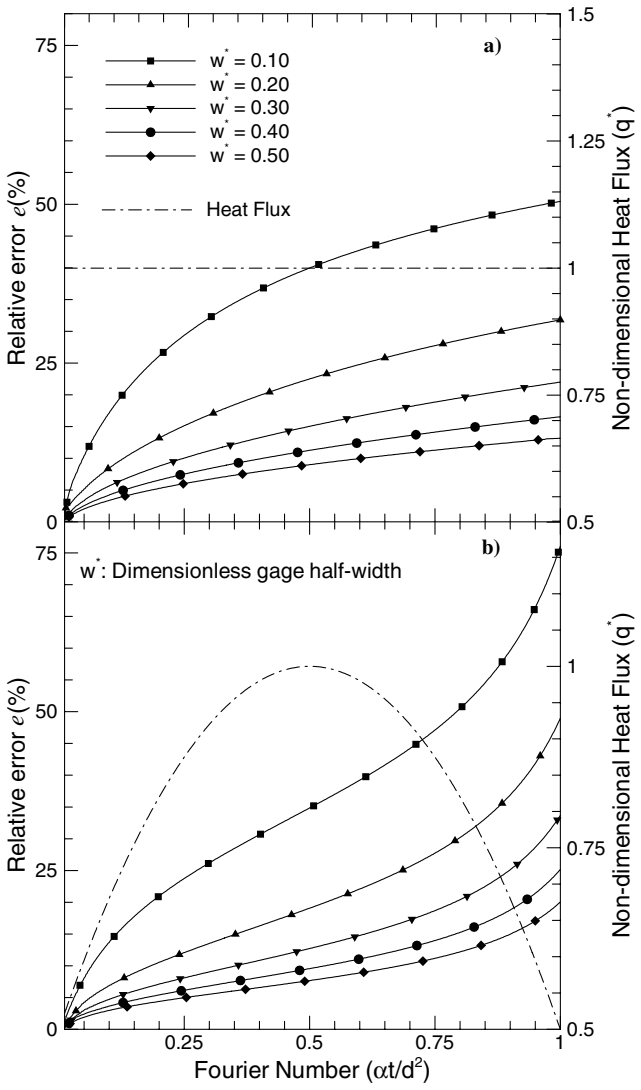

Fig. 9 Effect of Fourier number on relative error e for different dimensionless gage half-widths with a) a constant heat-flux profile, b) a parabolic heat-flux profile.

Fourier number for a given τ_{max} and w^*; a decreasing heat-flux profile further escalates this tendency.

To understand the variation of e with the nature of input flux profile, a series of simulations are conducted using several monotonically varying heat-flux profiles. Six different profiles, labeled as C through H in Table 2, are used for this purpose with a constant w^* of 0.50. All simulations continue to $\tau_{max} = 1$. The resulting e variations with τ, along with input profiles, are plotted in Fig. 10. The results clearly reveals a sharp increase of e with temporally decreasing fluxes, while a moderate and largely profile-independent e variation for temporally increasing fluxes. For temporally decreasing fluxes, trends show that a lower heat flux produces larger e at a particular τ, and e rapidly increases as the flux approaches zero. For temporally increasing fluxes, however, e depends largely upon the heat-flux gradient ($dq^*/d\tau$), and a lower gradient produces a larger e. In Fig. 10, gradients of flux profiles F and H varies linearly with τ. However, gradient of profile F increases from 0 ($\tau = 0$) to 1 ($\tau = 1$), whereas that of profile H decreases from 1 to 0, intersecting each other at $\tau = 0.50$. Consequently, the relative error e from flux profile F exceeds that of profile H up to $\tau \approx 0.60$, after which the trend reverses. However, for all six cases, a temporally increasing heat flux produces a lower e than a temporally decreasing flux. Surface cooling experiments are, therefore, more prone to a 2-D effect than that of surface heating.

In many experiments, knowledge of the peak heat flux is of importance. Duration also sometimes poses a critical issue in

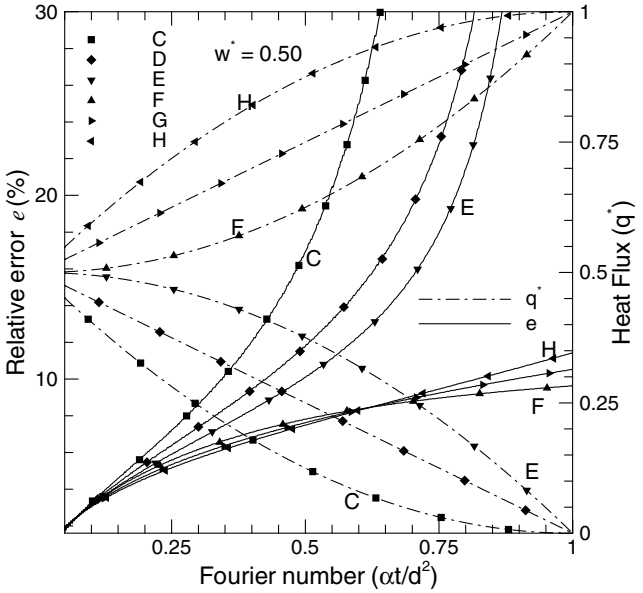

Fig. 10 Effect of Fourier number on the relative error e for different heat-flux profiles. Profiles C–E represent a temporally decreasing, whereas profiles F–H represent a temporally increasing flux.

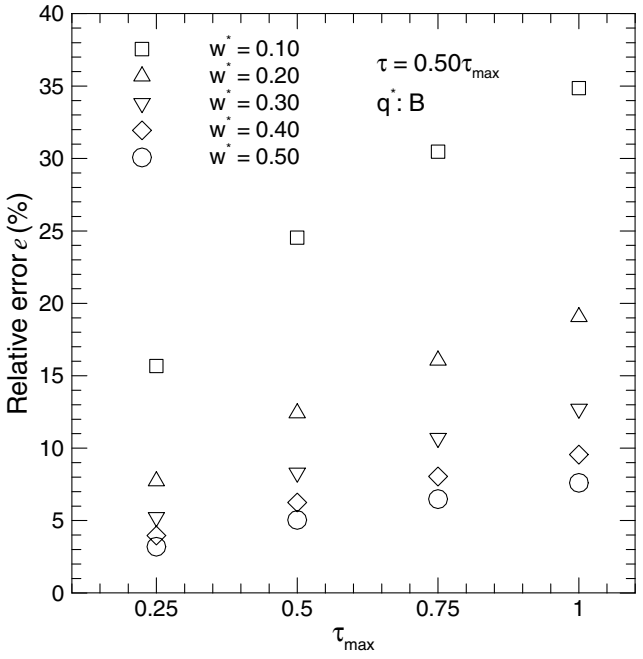

Fig. 11 Effect of maximum Fourier number on relative error e for different gage half-widths. Errors are calculated at the peak of a parabolic heat-flux profile.

designing an experiment. A series of simulations with varying w^* and τ_{max} are, therefore, conducted to address these questions. Results plotted in Fig. 11 show the variation of e at the peak flux location with τ_{max}. These results are generated with flux profile B. The 2-D effects are calculated at $\tau = 0.50\tau_{max}$ and consequently plotted against τ_{max}. Results show linear increase of e with τ_{max}. A maximum Fourier number of 0.50 will produce a 2-D effect of less than 25% at the point of peak heat flux.

Figure 12 shows variation of e at a particular τ with variable τ_{max}. Simulations with flux profiles A and B are conducted and corresponding 2-D effects at $\tau = 0.10$ are plotted against varying τ_{max}. Figures reveal the constancy of e with τ_{max} and independence of e on flux profiles for $w^* \geq 0.20$. With profile B, heat flux at $\tau = 0.10$ decreases with τ_{max}, producing a slightly increasing e [Fig. 12b]. For a constant heat flux (profile A), however, e decreases marginally.

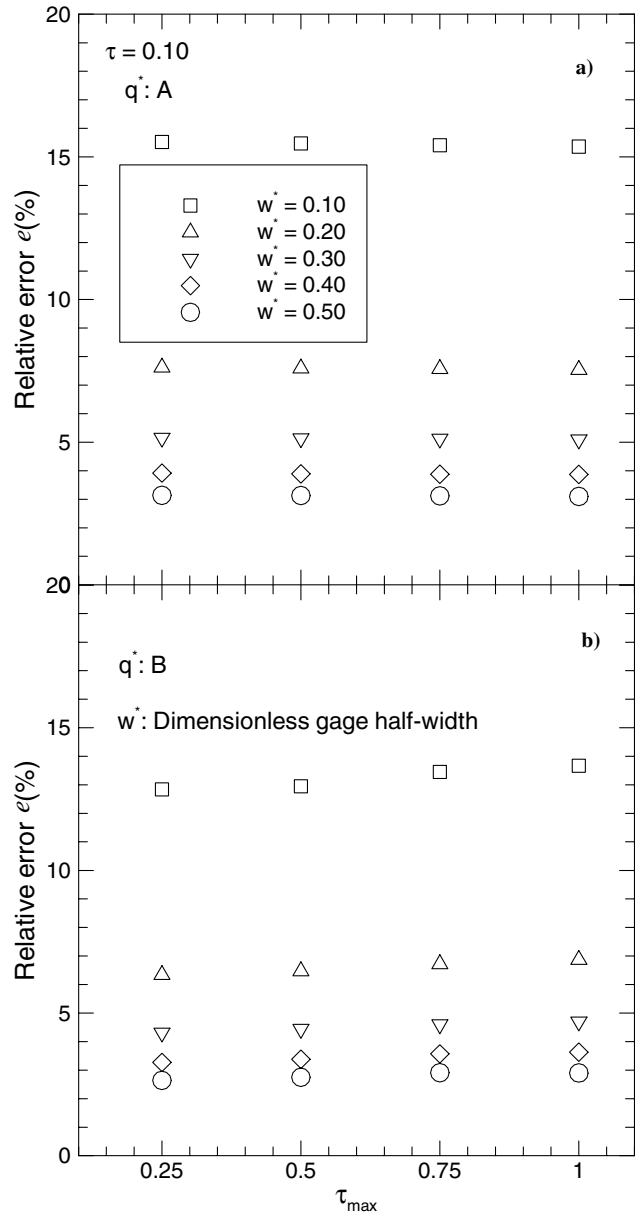

Fig. 12 Effect of maximum Fourier number on relative error e for different gage half-widths. Errors are calculated at a Fourier number of 0.10 with a) a temporally constant heat-flux profile, b) a parabolic heat-flux profile.

Results shown in Figs. 9–12 can serve as a guideline in designing experiments with thin-film heat-flux gages. Caution, however, should be exercised while using these figures or procedure for several reasons. First, these results used simulated temperature profile representing practically unattainable noise-free experimental data. Second, a real experiment can hardly produce a smoothly varying well-behaved transient flux profile. In the present experiment of plasma radiation, simulation with profile B predicts a 2-D effect of around 10% for sapphire and around 3% for polyimide, which are about 50% of the actual values shown in Table 3. A more realistic assumption of flux profile and noise level as well as a detail and quantitative error analysis will result in improved and more accurate design of an experiment.

Conclusions

Effects of 2-D heat conduction in estimating transient heat-flux profiles from surface temperature measurements are discussed. The major findings from this study are as follows:

1) Both 1-D and 2-D inverse techniques accurately recover the essential transient features in the heat flux, which are largely caused by compressible effects on temperature and species distributions within the plasma jet.

2) The importance of 2-D heat conduction increases nonlinearly with Fourier number and is largely independent of the heat-flux profile.

3) 2-D heat conduction effects are more significant for temporally decreasing heat-flux profiles than the increasing ones.

4) When measured at a fixed Fourier number, 2-D heat conduction effects remain largely independent of the maximum Fourier number as well as the nature of imposed heat-flux profiles.

The present study deals with the effects of data-reduction techniques in quantifying radiative heat transfer from a capillary-sustained plasma jet. Future studies will consider the effects of thermophysical and radiative properties of the substrate, film and window materials as well as the effect of nonzero film thickness on the radiative heat-flux estimation.

Acknowledgements

This work was supported by the U.S. Army Research Laboratory and the U.S. Army Research Office under Contract DAAD19-03-1-0340 with the management of Kevin McNesby. Equipment support from Kevin White and Richard Beyer of the Army Research Laboratory is greatly appreciated.

References

[1] Seymour, P. J., "Techniques for Numerical Evaluation of Unsteady Heat Flux From Thin Film Gauges," M.S. Thesis, State University of New York, Buffalo, New York, 1987.

[2] Taler, J., "Theory of Transient Experimental Techniques for Surface Heat Transfer," *International Journal of Heat and Mass Transfer*, Vol. 39, No. 17, 1996, pp. 3733–3748.

[3] Walker, D. G., and Scott, E. P., "One Dimensional Heat Flux History Estimation from Discrete Temperature Measurements," *Proceedings of ASME Heat Transfer Division*, Vol. 371, No. 1, American Society of Mechanical Engineers, New York, 1995, pp. 175–181.

[4] Walker, D. G., and Scott, E. P., "Evaluation of Estimation Methods for High Unsteady Heat Fluxes from Surface Measurements," *Journal of Thermophysics and Heat Transfer*, Vol. 12, No. 4, 1998, pp. 543–551.

[5] Ehrich, F. F., "Differentiation of Experimental Data Using Least Squares Fitting," *Journal of the Aeronautical Sciences*, Vol. 22, Feb. 1955, pp. 133–134.

[6] Jordan, P. F., "Differentiation of Experimental Data," *Journal of the Aeronautical Sciences*, Vol. 21, June 1954, pp. 417–418.

[7] Beck, J., Blackwell, B., and St. Clair, C., Jr., *Inverse Heat Conduction: Ill-Posed Problems*, Wiley, New York, 1985.

[8] Alifanov, O. M., *Inverse Heat Transfer Problems*, Springer–Verlag, New York, 1994.

[9] Varhegyi, G., "Numerical Differentiation of Experimental Data," *Information Processing Letters*, Vol. 2, No. 1, 1973, pp. 24–25.

[10] Wang, C-T., and DeSanto, D. F., "Differentiation of Experimental Data by Means of Higher Order Finite-Difference Formulas," *Journal of the Aeronautical Sciences*, Vol. 20, Nov. 1953, pp. 792–793.

[11] Cullum, J., "Numerical Differentiation and Regularization," *SIAM Journal on Numerical Analysis*, Vol. 8, No. 2, 1971, pp. 254–265.

[12] Anderssen, R. S., and Guttmann, A. J., "A Rationale for Numerical Differentiation of Experimental Data," *Information Processing Letters*, Vol. 4, No. 2, 1975, pp. 48–50.

[13] Li, X-S., Yang, J., and Liu, H., "Differentiation of Noisy Experimental Data for Interpretation of Nonlinear Stress–Strain Behavior," *Journal of Engineering Mechanics*, Vol. 124, No. 7, 1998, pp. 705–712.

[14] Tikonov, A. N., Goncharsky, A. V., Stepanov, V. V., and Yagola, A. G., *Numerical Methods for the Solution of Ill-Posed Problems*, Kluwer Academic Publishers, Dordrecht, The Netherlands, 1990.

[15] Ozisik, M. N., and Orlande, H. R. B., *Inverse Heat Transfer: Fundamentals and Applications*, Taylor and Francis, New York, 2000.

[16] Jarny, Y., Ozisik, M. N., and Bardon, J. P., "A General Optimization Method Using Adjoint Equation for Solving Multidimensional Inverse Heat Conduction," *International Journal of Heat and Mass Transfer*, Vol. 34, No. 11, 1991, pp. 2911–2919.

[17] Liu, F. B., and Ozisik, M. N., "Inverse Analysis of Transient Turbulent Forced Convection Inside Parallel Plate Ducts," *International Journal of Heat and Mass Transfer*, Vol. 39, No. 12, 1996, pp. 2615–2618.

[18] Ho, C-H., and Ozisik, M. N., "Inverse Radiation Problem in Inhomogeneous Media," *Journal of Quantitative Spectroscopy and Radiative Transfer*, Vol. 40, No. 5, 1988, pp. 553–560.

[19] Sawaf, B., and Ozisik, M. N., "An Inverse Analysis to Estimate Linearly Temperature Dependent Thermal Conductivity Components and Heat Capacity of an Orthotropic Medium," *International Journal of Heat and Mass Transfer*, Vol. 38, No. 16, 1995, pp. 3005–3010.

[20] Orlande, H. R. B., and Ozisik, M. N., "Inverse Analysis for Estimating the Electron–Phonon Coupling Factor in Thin Metal Films," *Journal of Applied Physics*, Vol. 78, No. 3, 1995, pp. 1843–1849.

[21] Chantasiriwan, S., "Inverse Heat Conduction Problem of Determining Time-Dependent Heat Transfer Coefficient," *International Journal of Heat and Mass Transfer*, Vol. 42, No. 23, 1999, pp. 4275–4285.

[22] Bezuidenhout, J. J., and Schetz, J. A., "Heat Flux Determination Using Surface and Backsurface Temperature Histories and Inverse Methods," Paper No. 2001-3530, 2001.

[23] Mota, C. A. A., Mikhailov, M. D., Orlande, H. R. B., and Cotta, R. M., "Identification of Heat Flux Imposed by an Oxyacetylene Torch," AIAA Paper No. 2004-4374, 2004.

[24] Das, M., Thynell, S. T., Li, J.-Q., and Litzinger, T. A., "Transient Radiative Heat Transfer From a Plasma Produced by a Capillary Discharge," *Journal of Thermophysics and Heat Transfer*, Vol. 19, No. 4, 2005, pp. 572–580.

[25] Das, M., Thynell, S. T., Li, J.-Q, and Litzinger, T. A., "Material Dependence of Plasma Radiation Produced by a Capillary Discharge," *Journal of Thermophysics and Heat Transfer* (to be published).

[26] Smith, D. E., Bubb, J. V., Popp, O., Diller, T. E., and Hevey, S. J., "A Comparison of Radiation Versus Convection Calibration of Thin-Film Heat Flux Gauges," *Proceedings of ASME Heat Transfer Division*, Vol. 364, No. 4, American Society of Mechanical Engineers, New York, 1999, pp. 79–84.

[27] Walker, D. G., and Scott, E. P., "Effects of Lateral Conduction on Heat Flux Estimation from Surface Temperature Measurements," *Proceedings of ASME Heat Transfer Division*, Vol. 357, No. 3, American Society of Mechanical Engineers, New York, 1998, pp. 245–252.

[28] Walker, D. G., Scott, E. P., and Nowak, R. J., "Estimation Methods for Two-Dimensional Conduction Effects of Shock–Shock Heat Fluxes," *Journal of Thermophysics and Heat Transfer*, Vol. 14, No. 4, 2000, pp. 533–539.

[29] Walker, D. G., and Scott, E. P., "A Method for Improving Two-Dimensional High Heat Flux Estimates from Surface Temperature," AIAA Paper No. 1997-2574, 1997.

[30] Beyer, R. A., and Pesce-Rodriguez, R. A., "Experiments to Define Plasma-Propellant Interactions," *IEEE Transactions on Magnetics*, Vol. 39, No. 1, 2003, pp. 207–211.

[31] Fifer, R. A., Sagan, E. S., and Beyer, R. A., "Chemical Effects in Plasma Ignition," *IEEE Transactions on Magnetics*, Vol. 39, No. 1, 2003, pp. 218–222.

[32] Perelmutter, L., Sudai, M., Goldenberg, C., Kimhe, D., Zeevi, Z., Arie, S., Melnik, M., and Melnik, D., "Temperature Compensation by Controlled Ignition Power in SPETC Guns," *Proceedings of the 16th International Symposium on Ballistics*, Vol. 1, National Defense Industrial Association, Arlington, VA, 1996, pp. 145–152.

[33] Edwards, C. M., Bourham, M. A., and Gilligan, J. G., "Experimental Studies of the Plasma-Propellant Interface for Electrothermal-Chemical Launchers," *IEEE Transactions on Magnetics*, Vol. 31, No. 1, 1995, pp. 404–409.

[34] Birk, A., Del Guercio, M., Kinkennon, A., Kooker, D. E., and Kaste, P., "Interrupted-Burning Tests of Plasma Ignited JA2 and M30 Grains in a Closed Chamber," *Propellants, Explosives, Pyrotechnics*, Vol. 25, No. 3, 2000, pp. 133–142.

[35] Kim, J. U., Clemens, N. T., and Varghese, P. L., "Experimental Study of the Transient Underexpanded Jet Generated by Electrothermal Capillary Plasma," *Journal of Propulsion and Power*, Vol. 18, No. 6, 2002, pp. 1153–1160.

[36] Kappen, K., and Beyer, R. A., "Progress in Understanding Plasma-Propellant Interaction," *Propellants, Explosives, Pyrotechnics*, Vol. 28, No. 1, 2003, pp. 32–36.

[37] Li, J.-Q., Litzinger, T. A., and Thynell, S. T., "Interactions of Capillary Plasma with Double-Base and Composite Propellants," *Journal of Propulsion and Power*, Vol. 20, No. 4, 2004, pp. 675–683.

[38] Li, J.-Q., Litzinger, T. A., and Thynell, S. T., "Plasma Ignition and Combustion of JA2 Propellant," *Journal of Propulsion and Power*, Vol. 21, No. 1, 2005, pp. 44–53.

[39] Wren, G. P., Oberle, W. F., and Hosangadi, A., "Influence of Radiation on Grain Heating in ETC Closed Chambers," *IEEE Transactions on Magnetics*, Vol. 35, No. 1, 1999, pp. 234–239.

[40] Taylor, M. J., "Spectral Acquisition and Calibration Techniques for the Measurements of Radiative Flux Incident upon Propellant,"

Propellants, Explosives, Pyrotechnics, Vol. 28, No. 1, 2003, pp. 18–25.

[41] Ryan, M. D., Clemens, N., T., and Varghese, P. L., "Measurements of Electrothermal-Plasma Ignition of Solid Propellants," AIAA Paper No. 2004-0388, 2004.

[42] White, K., Williams, A. W., and Nusca, M., "Plasma Output and Propellant Radiation Absorption Characteristics," *Proceedings of 35th JANNAF Combustion Subcommittee Meeting*, edited by R. S. Fry and M. T. Gannaway, Chemical Propulsion Information Agency Publication 680, Vol. 1, Johns Hopkins Univ., Columbia, MD, 1998, pp. 237–246.

[43] Williams, A. W., and White, K., "Plasma-Propellant Interaction Studies: Measurements of Heat Flux Produced by Hydrocarbon Ablation-Supported Plasmas," *IEEE Transactions on Magnetics*, Vol. 37, No. 1, 2001, pp. 203–206.

[44] Williams, A. W., and Beyer, R. A., "Heat Flux Measurements of Plasmas," *Proceedings of 39th JANNAF Combustion Subcommittee Meeting*, edited by R. S. Fry and M. T. Gannaway, Johns Hopkins Univ., Columbia, MD, 2003; Paper No. 2003-03990AG [CD-ROM], 9 pages.

[45] Gruber, K., Kappen, K., Voronov, A., and Haak, H., "Radiation Absorption of Propellant Gas," *IEEE Transactions on Magnetics*, Vol. 37, No. 1, 2001, pp. 161–164.

[46] Kappen, K., and Bauder, U. H., "Calculation of Plasma Radiation Transport for Description of Propellant Ignition and Simulation of Interior Ballistics in ETC Guns," *IEEE Transactions on Magnetics*, Vol. 37, No. 1, 2001, pp. 169–172.

[47] Kappen, K., and Bauder, U. H., "Simulation of Plasma Radiation in Electrothermal-Chemical Accelerators," *IEEE Transactions on Magnetics*, Vol. 35, No. 1, 1999, pp. 192–196.

[48] Huang, C-H., and Wu, J-Y., "Two-Dimensional Inverse Problem in Estimating Heat Fluxes of an Enclosure with Unknown Internal Heat Sources," *Journal of Applied Physics*, Vol. 76, No. 1, 1994, pp. 133–141.

[49] Huang, C-H., and Wang, S-P., "Three-Dimensional Inverse Heat Conduction Problem in Estimating Surface Heat Flux by Conjugate Gradient Method," *International Journal of Heat and Mass Transfer*, Vol. 42, No. 18, 1999, pp. 3387–3403.

[50] Rao, S. S., *Engineering Optimization: Theory and Practice*, 3rd ed., Wiley, New York, 1996.

[51] Das, M. K., Tariq, A., Panigrahi, P. K., and Muralidhar, K., "Estimation of Convective Heat Transfer Coefficient from Transient Liquid Crystal Data Using an Inverse Technique," *Inverse Problems in Science and Engineering*, Vol. 13, No. 2, 2005, pp. 133–155.

[52] Kunisch, K., and Zou, J., "Iterative Choices of Regularization Parameter in Linear Inverse Problems," *Inverse Problems*, Vol. 14, No. 5, 1998, pp. 1247–1264.

[53] Huang, C-H., and Chen, W-C., "Three-Dimensional Inverse Forced Convection Problem in Estimating Surface Heat Flux by Conjugate Gradient Method," *International Journal of Heat and Mass Transfer*, Vol. 43, No. 17, 2000, pp. 3171–3181.

[54] Tannehill, J. C., Anderson, D. A., and Pletcher, R. H., *Computational Fluid Mechanics and Heat Transfer*, 2nd ed., Taylor and Francis, Philadelphia, 1997.

[55] Chan, T. L., Ashforth-Frost, S., and Jambunathan, K., "Calibrating for Viewing Angle Effect During Heat Transfer Measurements on a Curved Surface," *International Journal of Heat and Mass Transfer*, Vol. 44, No. 12, 2001, pp. 2209–2223.

[56] Kurabayashi, K., Asheghi, M., Touzelbaev, M., and Goodson, K. E., "Measurement of the Thermal Conductivity Anisotropy in Polyimide Films," *Journal of Microelectromechanical Systems*, Vol. 8, No. 2, 1999, pp. 180–191.

[57] Press, W. H., Tukolosky, S. A., Vetterling, W. T., and Flannery, B. P., *Numerical Recipes in FORTRAN 77: The Art of Scientific Computing*, 2nd ed., Cambridge University Press, New York, 1999.